

Thermodynamics of U(VI) sorption onto *Shewanella putrefaciens*

Johnson R. Haas^{a,*}, Thomas J. Dichristina^b, Roy Wade Jr.^b

^a Departments of Chemistry and Environmental Studies, Western Michigan University, Kalamazoo, MI 49008, USA

^b School of Biology, Georgia Institute of Technology, Atlanta, GA 30332-0230, USA

Abstract

We have conducted acid–base potentiometric titrations and U(VI) sorption experiments using the Gram negative, facultatively anaerobic bacterium *Shewanella putrefaciens*. Results of reversed titration studies on live, inactive bacteria indicate that their pH-buffering properties result from the equilibrium ionization of three discrete populations of functional groups. Carboxyl ($pK_a = 5.16 \pm 0.04$), phosphoryl ($pK_a = 7.22 \pm 0.15$) and amine ($pK_a = 10.04 \pm 0.67$) groups most likely represent these three resolvable functionalities, based on their pK_a values. Site densities for carboxyl, phosphoryl and amine groups on the bacterial surface were approximately $31.7 \mu\text{mol sites/g bacteria}$ ($0.35 \pm 0.02 \text{ sites/nm}^2$), $8.95 \mu\text{mol/g}$ ($0.11 \pm 0.007 \text{ sites/nm}^2$) and $38.0 \mu\text{mol/g}$ ($0.42 \pm 0.008 \text{ sites/nm}^2$), respectively, based on an estimated bacterial specific surface area of $55 \text{ m}^2/\text{g}$. Sorption experiments showed that U(VI) can reversibly complex with the bacterial surface in the pH 2–8 interval, with maximum adsorption occurring at a pH of ~ 5 . Sorption is not strongly sensitive to ionic strength (NaCl) in the range 0.02–0.10 M. The pH and ionic strength dependence of U(VI) sorption onto *S. putrefaciens* is similar to that measured for metal-oxide surfaces and Gram positive bacteria, and appears to be similarly governed by competitive speciation constraints. Measured U(VI) sorption is accounted for by using two separate adsorption reactions forming the surface complexes $>\text{COO}-\text{UO}_2^+$ and $>\text{PO}_4\text{H}-\text{UO}_2(\text{OH})_2$. Using *S. putrefaciens* as a model organism for dissimilatory metal-reducing Gram negative anaerobes, our results extend the applicability of geochemical speciation models to include bacteria that are capable of reductively solubilizing or precipitating a wide variety of environmentally and geologically important metals and metallic species. © 2001 Elsevier Science B.V. All rights reserved.

Keywords: *Shewanella putrefaciens*; Bacteria; Geomicrobiology; Uranium; Adsorption

1. Introduction

The majority of bacteria in the subsurface exist and grow anaerobically, respiring on a variety of terminal electron acceptors (TEAs) other than oxygen, including NO_3^- , Fe(III), Mn(IV), SO_4^{2-} (Madigan et al., 2000), trace species U(VI), Se(IV), As(V), Cr(VI) (Winkler et al., 1995; Wade and DiChristina, 2000; Taratus et al., 2000) and exotic species such as Tc(VII) (Lloyd et al., 1998, 1999) and possibly

Pu(V,VI) (Rusin et al., 1994). Dissimilatory anaerobic bacteria that respire using oxidized metals must obtain energy by coupling the enzymatic reduction of Fe(III), Mn(IV) or other species to the oxidation of organic matter (Lovley, 1991; Nealson and Safarini, 1994). However, unlike dissolved oxygen, nitrate or sulfate, the predominant aquatic Fe(III) and Mn(IV) species are relatively insoluble metal-oxide phases. Thus, anaerobic metal-reducing bacteria (MRB) are typically faced with a physiological problem; oxidized metal species that are needed for respiration are encountered in a solid form that is not readily amenable to uptake via simple diffusion

* Corresponding author. Fax: +1-616-387-2909.
E-mail address: jhaas@wmich.edu (J.R. Haas).

across the cell membrane. In contrast, MRB that respire using soluble oxidized-metal species such as U(VI) (Lovley et al., 1991, 1993; Wade and DiChristina, 2000) may potentially acquire TEA ions through cross-membrane diffusion. Surface complexation represents a potentially more efficient mechanism by which bacteria may concentrate dissolved TEAs at the cell-aqueous or cell-mineral interface. MRB may facilitate this process by optimizing cell-surface properties to maximize the efficiency of ion acquisition or cell-mineral attachment. Quantification of the chemical thermodynamic properties of MRB cell walls should therefore promote a much clearer understanding of the importance of MRB in the biogeochemical cycling of metals, Fe and Mn mineral formation and dissolution, and the speciation, mobility and bioavailability of redox-sensitive chemical contaminants.

Several recent studies have sought to quantify the phenomenon of solute adsorption onto microbial surfaces, focusing primarily on the chemical thermodynamics of coordination onto Gram positive aerobic bacteria such as *Bacillus* sp. (e.g. Fein et al., 1997; Daughney et al., 1998; Fein and Delea, 1999; Fowle and Fein, 1999). For example, Fowle et al. (2000) demonstrate that U sorption onto *B. subtilis* can be described using a multisite surface complexation approach and report that U sorption onto that bacterium is governed by the formation of U-carboxyl and U-*H*-phosphoryl surface species. The stability constants obtained by Fowle et al. (2000) and others can be used to predict the speciation of solutes in oxygenated ground waters where aerobic Gram positive species similar to *Bacillus* are abundant. However, Gram positive and negative bacteria differ significantly in their cell membrane structures and compositions. Studies focusing on Gram positive species can provide only limited information regarding the coordination properties of Gram negative strains. Most bacteria in marine and freshwater settings are Gram negative (Hodgkiss and Shewan, 1968). MRB and sulfate-reducing bacteria (SRB), predominantly Gram negative Bacteria or Archaea (Barns and Nierzwicki-Bauer, 1997), are thought to be predominant in anoxic marine, estuarine and lacustrine systems where sulfate or metal-oxide minerals are abundant (Lee, 1979; Nealson and Stahl, 1997). Gram negative dissimilatory MRB such as *Shewanella* and

Geobacter are widespread in aquatic and marine systems and are thought to govern the global biogeochemical iron cycle (Nealson and Stahl, 1997).

In this study, we present potentiometric titration and U(VI) adsorption measurements made using *S. putrefaciens* strain 200R (Obuekwe et al., 1981; MacDonell and Colwell, 1985; DiChristina and DeLong, 1994). These data were used with a constant capacitance surface complexation model to derive standard state thermodynamic stability constants for protonation, deprotonation and U(VI) adsorption at the bacterial cell wall. We have selected *S. putrefaciens* as a model organism representing a dissimilatory Gram negative MRB found in a wide variety of aquatic settings. U(VI) is a widespread environmental contaminant in ground and surface waters, and can be enzymatically reduced to U(IV) by *S. putrefaciens* (Lovley et al., 1991; Wade and DiChristina, 2000).

2. Structure and acid–base chemistry of the Gram negative cell envelope

The cell walls of Gram negative bacteria differ significantly from those of Gram positive species. The Gram positive cell envelope is characterized by a cytoplasmic membrane consisting of a phospholipid bilayer and associated wall proteins and enzymes, surrounded externally by a thick layer of peptidoglycan (PG) or murein, a biopolymer consisting of peptide-cross-linked *N*-acetylglucosamine and *N*-acetylmuramic acid. The PG layer is studded with wall-associated proteins and teichoic and lipoteichoic acid derivatives which presents a surface that is rich with acid functional groups that deprotonate in pH-neutral aqueous solutions to yield a net negatively charged surface electric field (Beveridge and Koval, 1981; Beveridge et al., 1982; Beveridge and Fyfe, 1985; Schultze-Lam et al., 1995; Fortin et al., 1997; Madigan et al., 2000).

Gram negative cells also possess a cytoplasmic envelope consisting of a phospholipid bilayer surrounded by a PG layer. However, in Gram negative cells the PG layer is much thinner than what is typical for Gram-positive species, and is found in the periplasmic space between the underlying cytoplasmic membrane and an overlying outer membrane. This outer membrane is anchored to the PG layer by

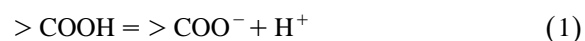
lipoprotein molecules, which are in turn linked to the overlying inner aspect of the outer-membrane phospholipid bilayer. The outer-membrane bilayer is traversed by proteins and porin channels that link the outer membrane to the periplasmic space and allow the exchange of low-molecular-weight chemical species between the cytoplasm and the external environment. The outer aspect of the outer membrane is composed largely of lipopolysaccharide (LPS), which is thought to play an important role in metal binding to the cell exterior (Langley and Beveridge, 1999). Structurally, LPS consists of a basal lipid A component linked to a core polysaccharide complex that projects from the lipid A matrix. Ketodeoxyoctonate (KDO) links the core polysaccharide to lipid A, which in turn is linked to a chain-like arrangement of heptoses, glucose, galactose, and *N*-acetylglucosamine that projects into the aqueous medium. The distal end of this strand consists of *O*-polysaccharide, containing galactose, glucose, rhamnose, mannose and other sugars in a branched repeating sequence (Madigan et al., 2000). *O*-polysaccharide varies in structure and composition among strains and thus acts as a serological antigen unit.

S. putrefaciens LPS has been characterized (Moule and Wilkinson, 1989). By weight, fatty acids are its most abundant components, consisting of linear and branched 11- to 15-carbon fatty acids, most of which possess three hydroxyl groups. Fatty acids contribute as the predominant fraction of carboxylic groups associated with LPS in this bacterium, although absolute abundances of ionizable groups are difficult to extract since the majority of LPS fatty-acid carboxyl groups are occupied in ester linkages. Carbohydrates and sugars contribute the second-most abundant source of potentially ionizable LPS functionalities in the form of hydroxyl groups on sugars. A number of these OH groups may remain ionizable even though the sugar units are linked in polysaccharide and carbohydrate chains. For example, a six-carbon-saccharide carbohydrate chain will yield two OH groups per repeating six-carbon sugar. Amino compounds comprise the third-most abundant source of ionizable functional groups in LPS, including glucosamine, galactosamine and similar amino-compounds. These components provide one amine group per molar unit, but like the carboxyl contribution to LPS many amines will tend to be occupied in peptide bonds and

thus may not be ionizable. However, an additional source of ionizable amine groups may be found in proteins, enzymes and porins associated with the outer aspect of the cell membrane. These molecules present a variety of ionizable groups in solution, most notably carboxyl and amine groups, with a lesser contribution by other groups such as phenolic (i.e. tyrosine) and sulfhydryl (i.e. cysteine) moieties (Voet and Voet, 1995). Phosphate represents a minor LPS component, found primarily in the core polysaccharide complex, but because most phosphate groups are found as terminal units this functional group may provide a significant source of ionizable groups.

3. Theoretical depiction of chemical interactions at the cell envelope

The aggregate of ionizable groups associated with the cell surface will contribute an overall electrical charge that will vary in magnitude with pH and ionic strength of the aqueous medium. Describing the pH and compositional dependence of the overall electrical field exhibited by the cell surface is facilitated by the application of chemical thermodynamic principles. In this approach, the overall properties of the cell surface are quantified in terms of discrete mass-law and mass-action equations that account for variations in charge density and metal coordination with pH and fluid compositions. Possible mass-law expressions accounting for surface charge on bacterial cell walls include



which represent carboxyl, amine and phosphoryl ionization reactions, respectively. In each of reactions (1) through (3), the symbol “>” indicates the binding point of each functional group to the remainder of its respective biomolecule. Reactions involving surface functional groups may be described using mass-action relations, which for Eq. (1), for example, will take the form

$$K = \frac{[> \text{COO}^-][\text{H}^+]}{[> \text{COOH}]} \quad (4)$$

where K represents the apparent equilibrium constant for reaction (1). Because these reactions take place on the surface, their physical–chemical depiction must account for electrostatic effects that will tend to modify the chemical thermodynamic relation. Including an electrostatic term in relation (4) yields

$$K = K_{\text{int}} \exp\left(-\frac{\Delta ZF\Psi_0}{RT}\right) \quad (5)$$

where K_{int} stands for the intrinsic equilibrium constant for the reaction at a condition of zero net surface charge and zero surface concentration of the adsorbing ion (H^+), ΔZ represents the change in charge of the adsorbing ion, F is the Faraday constant, Ψ_0 stands for surface electrical potential, R is the gas constant and T is temperature in Kelvin (Stumm and Morgan, 1996). In this study we describe the electrical potential near the cell surface using a constant capacitance model of the electrical double layer, wherein capacitance C is related to the surface electrical potential and surface charge σ by the following relation:

$$C = \frac{\sigma}{\Psi_0} \quad (6)$$

A constant capacitance model is used to describe the surface of *Bacillus* sp. by Fein et al. (1997), Daughney et al. (1998), Fein and Delea (1999), Fowle and Fein (1999) and Fowle et al. (2000) and a similar approach was used in this study to yield values that may be compared directly with previously published data describing bacteria–solute interactions. A capacitance of 1.0 F/m^2 for the *S. putrefaciens* surface was used in this study, based on the recommended value of Sahai and Sverjensky (1997) for capacitance for the inner Helmholtz layer of mineral surfaces in a NaCl solution. Results obtained in this study from modeling titration data were not particularly sensitive to values of C , therefore a value of 1.0 F/m^2 was selected and used for all calculations presented here.

4. Uranium geochemistry

Uranium occurs predominantly in two valence states under natural conditions, as U(VI) and U(IV). U(VI) hydrolyzes in solution to form the aquo-

ation complex UO_2^{2+} or uranyl. U(IV) occurs as the aquo cation U^{4+} . Both valence states strongly complex anions and ligands forming a diverse suite of aqueous complexes. Most notably, UO_2^{2+} readily complexes with dissolved carbonate, phosphate, hydroxyl and carboxylic acid ligands (e.g. Wagman et al., 1982; Tripathi, 1984; Grenthe et al., 1992; Shock and Koretsky, 1993, 1995; Ticknor et al., 1996; Prapaipong et al., 1999). High ligand concentrations promote U solubility via chelation reactions, but can also result in immobilization of U(VI) through chelation or adsorption onto colloidal organic matter (Read et al., 1993), onto mineral surfaces (Ho and Miller, 1985, 1986; Gabriel et al., 1998) or through precipitation of a variety of carbonate, sulfate, phosphate and arsenate minerals. Adsorption of U(VI) by mineral and organic substrates can also remove U(VI) from solution. Experimental and field studies by Moulin and Ouzounian (1992), Kohler et al. (1996), Hsi and Langmuir (1985), Ho and Doern (1985), Sagert et al. (1989), Sheppard and Thibault (1992), Prikryl et al. (1994), Bruno et al. (1995), Waite et al. (1994), Haas et al. (1998) and others have demonstrated that sorption of U(VI) onto mineral and biomass surfaces can extract nearly 100% of aqueous U(VI) at realistic environmental concentrations, and that this process is highly pH-dependent. At pH values below ~ 3 , U(VI) sorption is minimal, while sorption increases to a maximum through the pH interval ~ 3 – 7 , forming a characteristic “edge” on diagrams of pH versus extent of sorption. At pH values above ~ 7 – 8 , competition for U(VI) with aqueous carbonate and hydroxide reduces the extent of sorption, resulting in the release of U(VI) back to solution at increasingly basic pH values.

5. Experimental methods

5.1. Cultivation methods

S. putrefaciens strain 200R (Obuekwe et al., 1981; DiChristina and DeLong, 1994) was used in all experiments in this paper. Cultures were grown at 30°C in liquid Luria Bertani (LB) medium in the presence of $100 \mu\text{g/ml}$ rifamycin under anaerobic conditions. 200R is a spontaneous rifamycin-resistant strain. *S. putrefaciens* cultures were grown to mid-

logarithmic stage before harvest. Cell densities at extraction were measured using UV-visible spectrophotometry. Under invariant growth conditions, absorbency of cell suspensions at 600 nm correlates with cell density and growth stage (DiChristina, 1989). At harvest, cells were treated with 25 $\mu\text{g}/\text{l}$ of the antibiotic chloramphenicol. The principal effect of chloramphenicol on *S. putrefaciens* is to arrest the synthesis of new proteins. Chloramphenicol treatment was thus used in this study as a means of preventing subsequent cell growth or the expression of new proteins by viable cells during experiments. Harvested cells were separated from their growth media through a repeated centrifugation and resuspension procedure that was duplicated for all cell crops. The wash procedure involved centrifugation at $5000 \times g$ for 10 min to pelletize the cell mass, after which the supernatant was discarded and the pelletized cell mass was resuspended in 0.1 M NaCl electrolyte solution and concentrated by a factor of four from the original incubation volume. Cells were then centrifuged again for 10 min at $5000 \times g$, the supernatant discarded and the cell pellet resuspended in 0.1 M NaCl without additional concentration.

Cell densities in final 0.1 M NaCl solutions were counted via epifluorescence microscopy (Nikon Daiphot 300 microscope) using an acridine orange direct count (AODC) method (Lovley and Phillips, 1988). Cell suspensions in 0.1 M NaCl were used immediately in experiments or maintained at 4 °C for no longer than 1 week. In other studies (e.g. Fein et al., 1997; Daughney et al., 1998; Fein and Delea, 1999; Fowle and Fein, 1999) of Gram positive bacteria, chemical treatments with EDTA or strong acid were used to remove adsorbed cationic species from cell membranes. In this study no such chemical treatments were used to avoid damaging structural molecules of the LPS layer. The LPS layer can be altered or damaged by chemical treatments including EDTA (Birdsell and Cota-Robles, 1967; Costerton et al., 1967; Costerton, 1970), resulting in detachment of cationic cross-links between LPS strands and shortening of LPS units.

5.2. pH titrations

Acid–base titrations of *S. putrefaciens* were performed in an electronic titration apparatus (Mettler

Toledo model DL-58) at 25 °C. Solutions to be titrated were prepared using stock suspensions of *S. putrefaciens* with known cell density, which were diluted to desired experimental cell densities in a background electrolyte solution of 0.1 M NaCl. The total mass of cells used in each titration was approximated from measured cell density values using the growth data of DiChristina (1989) for *S. putrefaciens*. DiChristina (1989) report an average *S. putrefaciens* mass of 10^{12} bacteria/g under a range of growth conditions. Solutions to be titrated were dispensed into polypropylene vessels and secured to the burette assembly, then subsequently purged with N_2 gas to exclude atmospheric CO_2 for 1 h before the beginning of each titration. Control titrations with distilled-deionized water (DDW) showed that nitrogen purging was effective in removing dissolved CO_2 after approximately 15 min, determined via an observed elevation of fluid pH from a starting value of ~ 5.6 (representing equilibration with atmospheric CO_2) to ~ 7.0 . Fresh titration-grade 0.1 M NaOH and 0.1 M HCl (Titristar) standard solutions were used for titration experiments. Titrant standard solutions were calibrated against potassium hydrogen phthalate (for NaOH) and TRIS (for HCl). Titrations were performed by first allowing a given cell suspension to attain pH equilibrium to a drift of less than 0.1 mV (~ 0.001 pH unit)/10 s, then initiating an acid titration to an end-point of pH 3.0, followed by a base titration from pH 3.0 to an end-point of pH 10.0, followed by a second (reversed) acid-titration to an end-point of pH 3.0. Hysteresis of titration data was minimal and titrations appeared to be fully reversible. Titrations were performed by instrumental addition of titrant, in volumes of 10.0 μl , after achieving a pH drift at each step of equal to or less than 0.1 mV/10 s. Titrant volumes were accounted for in calculating dilution factors. The total volume of titrant delivered during each titration series was less than 2% of initial solution volume.

5.3. Surface area estimation

The wet surface area of *S. putrefaciens* was estimated in this study using a geometric approach. The external dimensions of viable bacteria were measured in photomicrographs obtained with scanning electron microscopy (SEM). The measured av-

erage long and short axes of *S. putrefaciens* were 1.92 ± 0.32 and 0.38 ± 0.09 μm , respectively, yielding an average aspect ratio of ~ 5.1 . We calculated the volume of a cylindrical *S. putrefaciens* bacterium to be 0.367 ± 0.07 μm^3 and the surface area to be 5.48 ± 1.0 μm^2 . He and Tebo (1998) found that BET estimates of surface area for freeze-dried bacterial spores underestimated the wet surface area, obtained through dye-adsorption experiments, by roughly an order of magnitude. Using a wet/dry surface area ratio of ~ 10 and a cell mass of 10^{12} bacteria/g (DiChristina, 1989) yields a specific surface area of approximately 55 m^2/g for wet *S. putrefaciens* bacteria. This value is similar to previous estimates of wet surface area for viable *Bacillus* sp. cells (140 m^2/g ; Fein et al., 1997) and spores (75 m^2/g ; He and Tebo, 1998) obtained using a combination of geometric, gas-adsorption and aqueous dye-adsorption methods.

5.4. UO_2^{2+} sorption experiments

Stock cell suspensions of inactive, viable *S. putrefaciens* were diluted with 0.1 M NaCl to desired concentrations and titrated with trace metal grade NaOH and HCl to desired pH values. Aliquots were extracted at desired pH conditions, in volumes of 4.0 ml, and dispensed into 4.0 -ml polypropylene sample vials. Forty microliters of a 1.0 -mM UO_2^{2+} solution was added to each vial, yielding initially a solution of 10 μM U. Stock 1.0 mM U solutions were prepared by dilution and pH neutralization of an atomic absorption standard solution ($10,000$ mg U/l in 2% HNO_3) in DDW. Experimental solutions were allowed to equilibrate for 12 h at 25 $^\circ\text{C}$ while being mixed on a circular rotational shaker. Overnight equilibration was used to overcome any potential problems arising from slow adsorption kinetics. However, test experiments were conducted at 1 -h equilibration times (data not shown), which demonstrated that nearly 90% of potential U uptake was attained within the first hour of equilibration. Reversibility of U uptake was tested by randomly selecting a small number of experimental solutions and mildly acidifying them (to a pH of ~ 2 – 3) after 1 h of equilibration. Results of reversibility trials (not shown) indicated that the extent of U uptake and U acidification-release were similar. Controls were run

without bacteria to test for loss of U to the vessel walls; no systematic U loss was observed.

At the end of the trials, equilibrium pH was measured using a glass-combination semimicro pH-electrode directly in experimental vessels. After pH measurements, aliquots were transferred to 1.5 ml centrifuge tubes and centrifuged at 8000 rpm in an Eppendorf microcentrifuge for 30 min. Supernatants were decanted into 15 ml polypropylene centrifuge tubes. After which, 20 μl of 6.0 M trace metal grade HNO_3 were added to each 15 -ml tube and the contents diluted to 10.0 ml with DDW. Resulting solutions were analyzed for U using inductively coupled plasma mass spectrometry (ICP/MS). Measured U concentrations reflected U not sorbed by bacteria during the experiments. In all experiments the availability of cell surface binding sites (see Section 6.2) was in excess of the U concentration. The low initial concentration of U (10.0 μM) was selected to avoid problems arising from $\text{UO}_2(\text{OH})_2(\text{s})$ (schoepite) precipitation or strong U loading of cell walls resulting in precipitation of Uranyl phases on bacteria, as was reported by Barker et al. (1998) and Suzuki and Banfield (1999) for lichen fungal cells.

6. Results

6.1. pH titrations

Fig. 1 displays sample titration curves for *S. putrefaciens* in 0.1 M NaCl electrolyte solution at three different cell densities. The net concentration of exchanged H^+ is calculated according to the following relation,

$$[\text{H}^+]_{\text{meas}} - [\text{OH}^-]_{\text{meas}} - [\text{H}^+]_{\text{added}} + [\text{OH}^-]_{\text{added}} = [\text{H}^+]_{\text{exchanged}} \quad (7)$$

where $[\text{H}^+]_{\text{meas}}$ and $[\text{OH}^-]_{\text{meas}}$ are obtained from the pH at each titration step, $[\text{H}^+]_{\text{added}}$ and $[\text{OH}^-]_{\text{added}}$ are known at each titration step, and the term $[\text{H}^+]_{\text{exchanged}}$ reflects the sum of all other proton exchange reactions in the system.

The titration curves in Fig. 1 are displayed in comparison to the calculated titration curve of pure water (dotted line) for a solution of identical volume

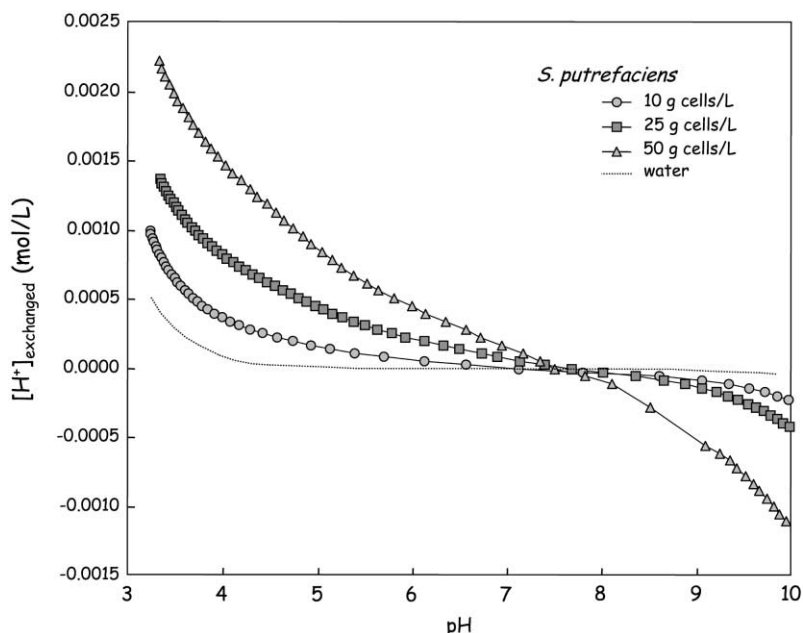


Fig. 1. Acid–base potentiometric titration data for *S. putrefaciens* at three different cell densities as a function of $[H^+]_{\text{exchanged}}$ and pH. Values of $[H^+]_{\text{exchanged}}$ are calculated using relation (7). A calculated titration curve for pure water is shown by the dotted line. Smoothed lines connect titration data points.

to the experimental solution. The curves for *S. putrefaciens* cross the titration curve for water near a pH of ~ 7.5 , indicating that the surfaces of *S. putrefaciens* cells are capable of gaining protons at low pH and acquiring a net positive charge. At pH values higher than ~ 7.5 , $[H^+]_{\text{exchanged}}$ is negative and the cell surface acquires a net negative charge. Previous studies of Gram positive bacteria of the genus *Bacillus* have reported that their cell membranes display a net negative charge at pH values greater than ~ 3.5 and are neutrally charged at lower pH values (Fein et al., 1997; Daughney et al., 1998). Those findings are consistent with the known composition of the outer aspect of Gram positive cell envelopes, which are comprised largely of PG and associated teichoic and lipoteichoic acids (Madigan et al., 2000) that display abundant carboxyl, phosphoryl and hydroxyl groups. Most studies assume that the outer surfaces of Gram negative bacteria behave similarly to Gram positives in regard to acid–base chemistry (Schultze-Lam et al., 1995), in that the cell surface is largely anionic. However, our titration results clearly demonstrate that the cell surface of *S. putrefaciens* is positively

charged at pH values more acidic than ~ 7.5 . At pH values higher than ~ 7.5 , cell surfaces become increasingly negatively charged strongly buffering pH up to the maximum titration pH ~ 10.0 . Interestingly, the optimal growth pH for *S. putrefaciens* is ~ 7.0 , at which the surface of this bacterium, according to titration data, will exhibit a slightly positive net charge. Under more basic conditions in most natural ground waters and in the oceans (pH ~ 8), our titration data indicates that *S. putrefaciens* will exhibit a slightly negative net charge, and thus adsorption of cations will not be electrostatically inhibited. However, in mildly acidic soils or in acidified ground waters the positive net charge of *S. putrefaciens* cell surfaces may significantly curtail cation-adsorption reactions. Conversely, ligand sorption at low pH is likely to be significant.

6.2. Thermodynamic modeling of titration data

The results of titration experiments were used to constrain an optimal description of the number, concentrations and thermodynamic properties of ioniz-

able functional groups on the *S. putrefaciens* surface. To facilitate the extraction of thermodynamic values from the titration data, the computer code FITEQL (Westall, 1982) was used to test the appropriateness of differing chemical mass-action and mass-law relations in describing the proton-exchange behavior of *S. putrefaciens* cell surfaces. FITEQL performs non-linear least squares regressions of experimental data using stoichiometric constraints supplied by the user. The quality of results obtained using FITEQL may be evaluated by direct comparison with observed experimental values and by seeking to minimize the sum of squares of residuals differential function (W_{sos}/df ; dimensionless) generated by the regression algorithm.

Specific adsorption of electrolyte ions to the bacterial surface was not accounted for computationally in this study. In order to reliably estimate the effects of electrolyte adsorption onto the bacterial surface, it would be necessary to conduct titration studies over a range of ionic strength values ideally covering several orders of magnitude in electrolyte concentration. This procedure is precluded on practical grounds because of the sensitivity of the bacterial surface to

extreme shifts in osmotic pressure and salt concentration. If exposed to ionic strengths significantly lower than that of their growth media (LB ~ 0.1 M NaCl) bacterial cells will tend to undergo spontaneous lysis, while at significantly higher ionic strengths membrane-mounted proteins will tend to solubilize (Voet and Voet, 1995; Madigan et al., 2000). For example, in NaCl an increase in ionic strength from ~ 0.1 to 1.0 will result in an increase in the solubility of carboxy-hemoglobin by approximately an order of magnitude (Voet and Voet, 1995). This “salting in” effect is routinely used in microbiology as a method of protein extraction. Titration data at NaCl ionic strengths of 0.1 and 0.05 were obtained in this study and the results are shown in Fig. 2. These results demonstrate that within a narrow range of ionic strength proton exchange at the bacterial surface is not measurably sensitive to electrolyte concentration, indicating that specific electrolyte adsorption by the bacterial surface is minimal.

Table 1 summarizes the results of FITEQL optimizations for one titration of *S. putrefaciens* (50 g cells/l), constrained according to a one acid-site model, a one base-site model, a one-site amphoteric

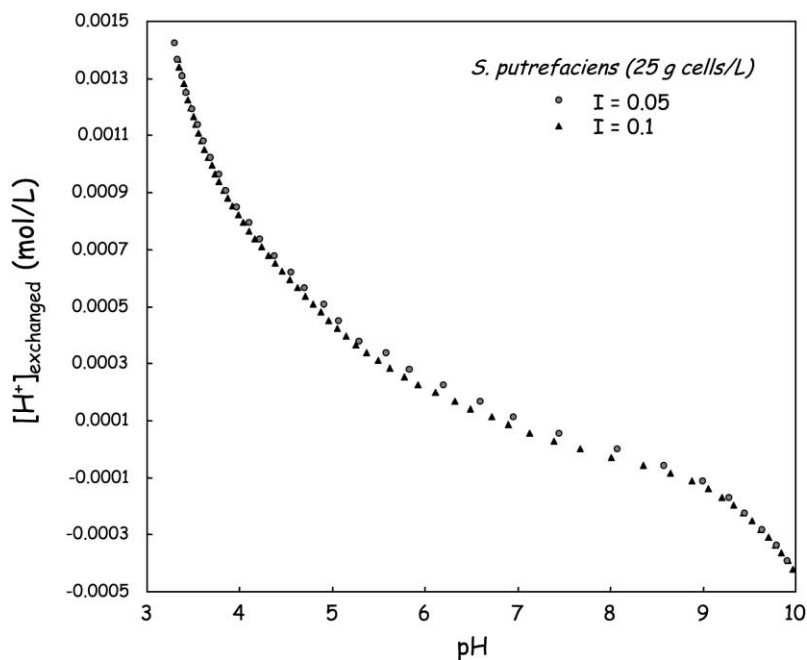


Fig. 2. Potentiometric titration curves for *S. putrefaciens* at 25 g bacteria/l and ionic strengths of 0.05 and 0.10 M NaCl.

Table 1

Results of FITEQL optimizations of differing constant-capacitance model stoichiometries representing the *S. putrefaciens* surface

A capacitance of 1.0 F/m² for the EDL was used in all calculations. W_{sos}/df values are sums of squares of residuals for each computation. N/C = no convergence. SD = site density in $\mu\text{mol sites/g}$ bacteria.

Sites: One acid			
Reaction:	$> \text{XH} = > \text{X}^- + \text{H}^+$		$W_{\text{sos}}/df:$ 1006
	$pK_a:$ 9.51		
	SD 45.8		
Sites: One base			
Reaction:	$> \text{YH}_2^+ = > \text{YH} + \text{H}^+$		$W_{\text{sos}}/df:$ 1881
	$pK_a:$ 5.70		
	SD 32.0		
Sites: One amphoteric			
Reaction:	$> \text{XH} = > \text{X}^- + \text{H}^+$	$> \text{XH}_2^+ = > \text{XH} + \text{H}^+$	$W_{\text{sos}}/df:$ 12.8
	$pK_a:$ 9.15	$pK_a:$ 5.75	
	SD 31.6		
Sites: One acid, one base			
Reaction:	$> \text{XH} = > \text{X}^- + \text{H}^+$	$> \text{YH}_2^+ = > \text{YH} + \text{H}^+$	$W_{\text{sos}}/df:$ 7.80
	$pK_a:$ 5.58	$pK_a:$ 8.98	
	SD 30.6	sites/nm ² : 32.8	
Sites: Two acid, one base			
Reaction:	$> \text{XH} = > \text{X}^- + \text{H}^+$	$> \text{YH}_2^+ = > \text{YH} + \text{H}^+$	$W_{\text{sos}}/df:$ 0.491
	$pK_a:$ 5.17	$pK_a:$ 9.37	
	SD: 9.96	SD: 37.4	
	$> \text{ZH} = > \text{Z}^- + \text{H}^+$		
	$pK_a:$ 7.06		
	SD: 29.4		

model, a two-site (acid-site and base-site) model, and a model involving two acid sites and one base site. The modeling procedure described here constrains the thermodynamic properties of the cell surface in statistical terms only and does not necessarily imply that regressed thermodynamic values describe the absolute properties of individual functional groups belonging to homogeneous populations on the cell surface. Rather, regressed properties for a particular reaction represent the average properties of a heterogeneous population of functional units, which collectively behave as if they were a single type of functionality. One test of this approach is whether it is even possible to describe acid–base reactions on the cell wall using such a discrete-reaction model. The cell surface, comprising a diverse suite of LPS components, wall proteins and enzymes, could in principle exhibit an assortment of functional groups whose properties are not collectively amenable to approximation as a small number of discrete site types, or which interact sterically as a function of pH, making the resolution of site properties difficult. The pH-

buffering properties of humic and fulvic acids, for example, normally cannot be resolved using a discrete multisite approach because of pH-dependent conformational shifts that shield or expose functionalities as they acquire or lose charge (Tipping and Hurley, 1992). However, the relative physical inflexibility of the bacterial cell and the highly structured nature of the cell envelope suggest that the cell surface should not behave like a humic acid, but more like a multifunctional organic acid or peptide. This expectation is confirmed by titration studies of Gram positive bacteria (Fein et al., 1997; Daughney et al., 1998), which show that a discrete multisite approach is applicable to *Bacillus* sp. bacteria.

Table 1 may be used to directly compare the quality of FITEQL-calculated fits to the experimental data shown in Fig. 3. The first model considered is the simplest; an approximation of the cell surface as a monoprotic acid with a pK_a . This one-acid-site model provides a poor fit to the titration data, yielding a high sum of squares of residuals ($W_{\text{sos}}/df = 1006$). This model fails to reproduce the titration

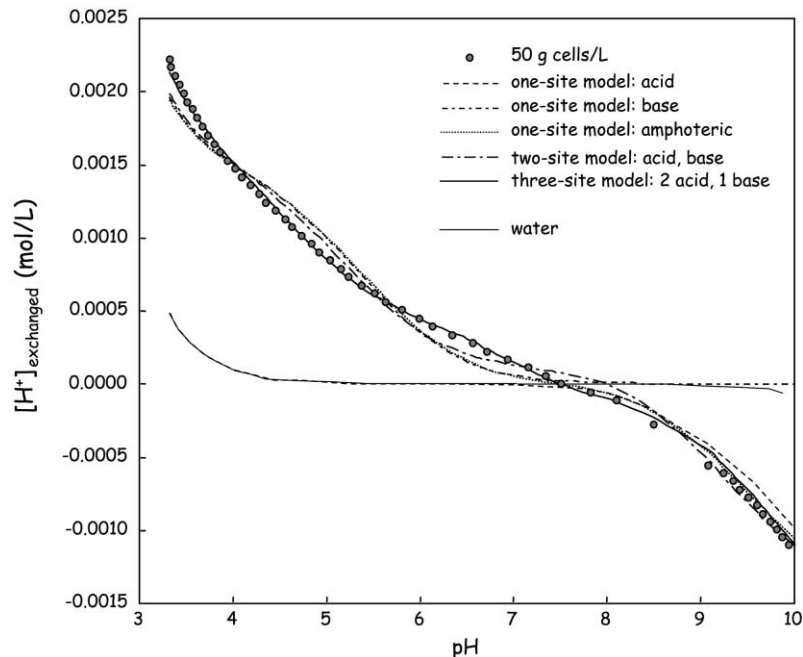


Fig. 3. Potentiometric titration curve for *S. putrefaciens* at 50 g bacteria/l. Also shown are FITEQL regressions (lines connecting data points) for different models of the cell surface.

data primarily because it cannot account for proton uptake by the surface under acidic pH conditions. A model involving only a proton-accepting or “base” site (i.e. relation (2)) also fails to adequately reproduce the titration data ($W_{\text{sos}}/df = 1881$) because it cannot account for proton buffering in the basic pH range. A single-site amphoteric model provides a substantially better fit to the experimental data ($W_{\text{sos}}/df = 12.8$) when compared with the one-acid-site or one-base-site models. A model separating the acid and base functions of the amphoteric model into two discrete sites accounts somewhat better for the titration data, yielding a W_{sos}/df value of 7.8.

A three-site model (two-acid-sites, one-base-site) provides a substantially improved fit ($W_{\text{sos}}/df = 0.491$) to the titration data when compared with previous models. Application of this model to the titration data at 10 and 25 g bacteria/l yields similar results in terms of pK_a values and absolute site concentrations, and also returns similarly low W_{sos}/df values (see Table 2). Fig. 3 compares all the models listed in Table 1 in terms of their correspondence with the titration data at 50-g bacteria/l.

The three-site model fits the experimental data more closely throughout the measured pH range than either the amphoteric or two-site models, while both the one-acid and one-base models yield titration curves that depart significantly from the experimental curve. Multisite models involving more than two sites (one acid and one base) fail to converge. Values obtained for titration results at three bacterial concentrations are shown in Table 2, along with averages of values from separate titrations. Average pK_a values obtained using the three-site model were (site > ZH) 5.16, (> XH) 7.22 and (> YH) 10.04, where ionization of >ZH and >XH obey a mass law similar to Eq. (1), and >YH obeys a mass law similar to Eq. (2). The estimated site concentrations obtained from the model were (> ZH) 31.7 μmol sites/g bacteria, (> XH) 9.85 $\mu\text{mol}/\text{g}$, and (> YH) 38.0 $\mu\text{mol}/\text{g}$.

6.3. Results of U sorption experiments

The results of U sorption experiments involving *S. putrefaciens* are shown in Fig. 4 as a function of

Table 2

Results of FITEQL calculations for individual titrations of *S. putrefaciens* in 0.1 mol/l NaCl, constrained according to a three-site model of the bacterial surface

pK_a values are calculated for proton-yielding reactions. Site densities assume a bacterial mass of 10^{12} bacteria/g. W_{sos}/df values are sums of squares of residuals computed by FITEQL.

g/l	pK_a (> XH)	$\mu\text{mol sites/g}$ (> XH)	pK_a (> YH)	$\mu\text{mol sites/g}$ (> YH)	pK_a (> ZH)	$\mu\text{mol sites/g}$ (> ZH)	W_{sos}/df
50	5.17	9.96	9.37	37.4	7.06	29.4	0.491
25	5.19	9.20	10.05	38.8	7.27	32.0	0.211
10	5.11	10.0	10.70	37.7	7.34	33.6	0.287
Average:	5.16	9.85	10.04	38.0	7.22	31.7	
Std:	0.04	0.61	0.67	0.74	0.15	2.1	

pH versus the percentage of available U taken up by the bacteria at two different ionic strengths and two different bacteria:U concentration ratios. Under highly acidic pH conditions U uptake is minimal (< 4% at pH 1.2). At pH values greater than ~ 2 U uptake increases, reaching 70–90% uptake at a pH of ~ 3 . Sorption reaches a maximum at a pH of ~ 4 –5 (95%+) and remains optimal up to a pH of ~ 6 –6.5, above which the extent of sorption diminishes as pH continues to rise. In the basic pH range the extent of sorption diminishes precipitously, drop-

ping to less than 20% at a pH of ~ 9 and below 5% at a pH of ~ 10 . Ionic strength effects appear to be minimal; an increase in NaCl ionic strength from 0.02 to 0.10 M appears to narrow the adsorption envelope only slightly. A similar result was obtained for U sorption onto hematite (Lenhart and Honeyman, 1999), which was interpreted to be consistent with the formation of inner-sphere U(VI)-hematite surface complexes (Hayes and Leckie, 1987).

The pH-dependence of U sorption shown in Fig. 4 is similar to that observed for U adsorption onto

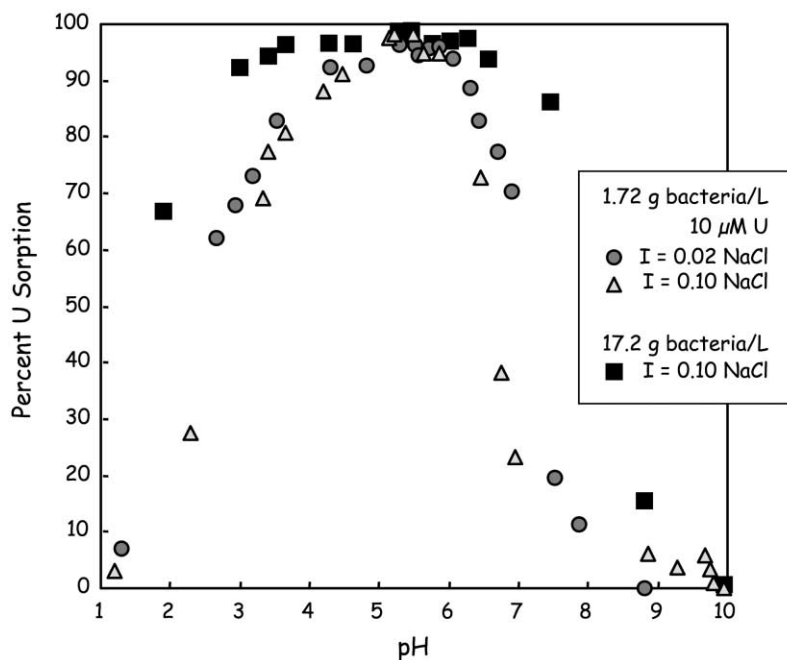


Fig. 4. Experimental data for U sorption onto *S. putrefaciens* as a function of pH, ionic strength and bacteria:U concentration ratio. Incubation time for all experiments was 12 h. Initial U concentration was 10 μM for all experiments.

ferrihydrate (Waite et al., 1994), hematite (Ho and Doern, 1985; Lenhart and Honeyman, 1999), and onto intact lichen biomass (Haas et al., 1998). A strong sorption edge for uranyl at low pH is characteristic of cation adsorption (Davis and Kent, 1990), while desorption of U at high pH results from strong complexation with carbonate and hydroxide anions at increasingly basic pH conditions. Under oxidizing and acidic pH conditions, the dominant form of U dissolved in water in equilibrium with atmospheric CO_2 is aquo-uranyl, but as pH increases to near-neutrality uranyl increasingly complexes to form a suite of hydroxide, carbonate and hydroxycarbonate neutral to anionic dissolved species (see Fig. 5). At increasingly basic pH values these complexes account for essentially all of available U, forming predominantly the species $\text{UO}_2(\text{CO}_3)_3^{2-}$ and $\text{UO}_2(\text{OH})_3^-$ at a U concentration of $10 \mu\text{M}$, $\text{pH} > 8$, and atmospheric $\text{CO}_2(\text{aq})$ concentrations (Tripathi, 1984; Grenthe et al., 1992). Lenhart and Honeyman (1999), Waite et al. (1994), Ho and Doern (1985) and Haas et al. (1998) demonstrate that this aspect of U sorption applies to a wide variety of surface types, including metal-oxide mineral surfaces and eukaryotic cell walls. The results shown in Fig. 4 indicate

that similar speciation constraints govern the adsorption of U by the cell envelope of *S. putrefaciens*.

6.4. Modeling U sorption equilibria

Data obtained from sorption experiments were used to constrain the properties of U adsorption onto the *S. putrefaciens* surface. FITEQL was used to carry out regression calculations testing the correspondence of different adsorption-reaction stoichiometries to the observed uptake data. Because of the complexity of U aqueous speciation and the wide range of pH conditions under which adsorption was measured in this study, complexation reactions forming a wide range of U hydroxide, carbonate, hydroxycarbonate and chloride complexes were included in the FITEQL speciation matrix. Species chosen for inclusion were selected based on their significance to U aqueous speciation in a homogeneous aqueous system. The aqueous speciation of U during our experiments (excluding bacteria) was calculated for an oxidizing solution (0.2 bar $\text{O}_2(\text{g})$) at 25°C and 1 bar, containing $10 \mu\text{M}$ U, $320 \mu\text{M}$ total dissolved CO_2 and 0.1 M NaCl, as a function of pH. Speciation calculations were performed using the computer

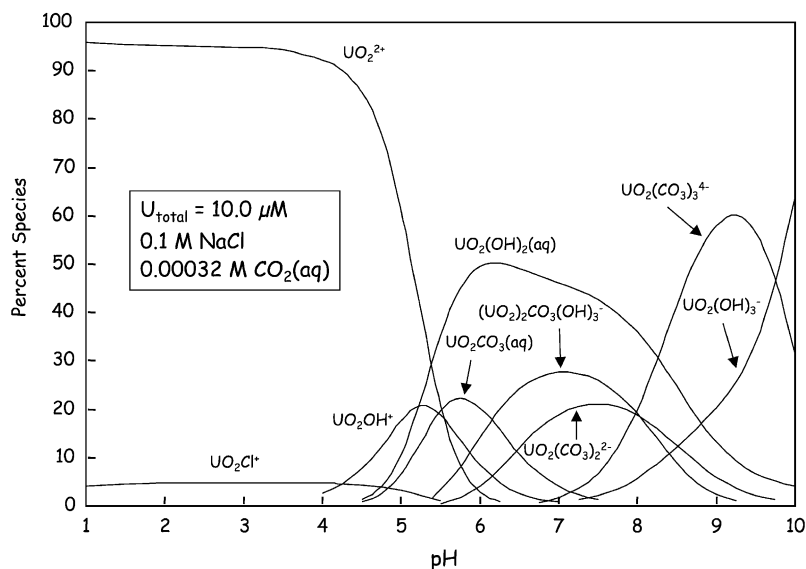


Fig. 5. Calculated U speciation profile as a function of pH. Solution composition: 0.2 bar $p\text{O}_2$, $U_{\text{total}} = 10 \mu\text{M}$, $\text{CO}_2(\text{aq}) = 3.2 \times 10^{-4} \text{ M}$, 0.1 M NaCl. Values were calculated using data of Grenthe et al. (1992) and Tripathi (1984).

code EQ3NR and its thermodynamic database (Wolery, 1992), which includes thermodynamic data of Tripathi (1984) and Grenthe et al. (1992) for U complexes.

Under the experimental conditions U is stable predominantly as U(VI) and is undersaturated with respect to schoepite ($\text{UO}_2(\text{OH})_2$), all dehydrated stoichiometric derivatives of schoepite ($\text{UO}_3(\text{OH})_X$ where $X \leq 1$), rutherfordine (UO_2CO_3), $\alpha\text{-UO}_3$, $\beta\text{-UO}_3$, and $\gamma\text{-UO}_3$. Aqueous U complexes that are significant under the experimental conditions are summarized along with their formation reactions and appropriate association constants in Table 3. Reactions selected include only those for which $\geq 1\%$ of aqueous U is accounted for by a given complex over a pH range of 0.5 log units or greater. Fig. 5 illustrates a speciation profile for U under the experimental conditions as a function of pH, calculated using the equilibria presented in Table 3.

The FITEQL speciation matrix used to regress properties of adsorption reactions included all reactions tabulated in Table 3, the autoionization of water, and dissociation reactions for HCl and NaOH. Activity coefficients for aqueous species were calculated by FITEQL using the Davies equation. Adsorption was constrained using the optimal three-site model of the *S. putrefaciens* surface, using average values for site densities and equilibrium constants of surface functional groups shown in Table 2. A summary of stoichiometric relations for U adsorption that were considered in this study are tabulated in Table 4, along with W_{sos}/df values generated by FITEQL for three sets of experimental U-sorption

data. As shown in Table 4 most of the reactions considered can account to some degree for the adsorption of U onto *S. putrefaciens*, but most cannot account successfully for the extent of sorption observed throughout the entire observed pH range or under all experimental conditions.

Models considered and listed in Table 4 include reactions sorbing U onto predicted carboxyl, phosphoryl, and amine sites at the bacterial surface. Stoichiometries for surface complexation involving protonated and deprotonated carboxyl, phosphoryl and amine sites were considered, including reactions coordinating uranyl-hydroxide (UO_2OH^+ , $\text{UO}_2(\text{OH})_2$, $\text{UO}_2(\text{OH}_3)^-$) and uranyl-carbonate (UO_2CO_3^0 , $\text{UO}_2(\text{CO}_3)_2^-$) species onto those surface groups. The most successful single-reaction stoichiometry involves bidentate adsorption of uranyl onto two deprotonated surface carboxyl groups, yielding low W_{sos}/df values under all three experimental conditions. However, regressed association constants for this reaction at different experimental conditions are significantly different from each other ($\log K = 2.4, 3.2, 4.5$). An average of these three values, when used to estimate the extent of U sorption by the bacteria as a function of pH, does not closely duplicate the experimental trends.

Models involving more than one type of surface complex generally account better for U sorption than do single-reaction models. The lower section of Table 4 lists a series of models that each include two separate adsorption reactions, and in most cases where model convergence is achieved the W_{sos}/df values obtained are smaller than that of the best of the single-reaction models. Some of the improvement is due to the increased number of fitting parameters in the two-reaction models. However, adding another reaction can only improve the quality of fit if a one-reaction model is inadequate, otherwise two postulated reactions will attain singularity and the model will fail to converge. All of the two-reaction models shown include the formation of a surface carboxyl-uranyl ($> \text{COO}-\text{UO}_2^+$) complex plus one other type of complex. Two-reaction combinations that did not include the $> \text{COO}-\text{UO}_2^+$ complex and combinations using three complexes or bidentate complexes either failed to converge or returned W_{sos}/df values significantly higher than those shown.

Table 3
Aqueous complexation equilibria and association constants ($\log K$) for UO_2^{2+} in experimental solutions (sans *S. putrefaciens*)
Sources: Tripathi (1994) and Grenthe et al. (1992).

Reaction	$\log K$
$\text{UO}_2^{2+} + \text{Cl}^- = \text{UO}_2\text{Cl}^+$	0.157
$\text{UO}_2^{2+} + \text{CO}_3^{2-} = \text{UO}_2\text{CO}_3^0$	9.67
$\text{UO}_2^{2+} + 2\text{CO}_3^{2-} = \text{UO}_2(\text{CO}_3)_2^{2-}$	16.91
$\text{UO}_2^{2+} + 3\text{CO}_3^{2-} = \text{UO}_2(\text{CO}_3)_3^{4-}$	23.63
$\text{UO}_2^{2+} + \text{H}_2\text{O} = \text{UO}_2\text{OH}^+ + \text{H}^+$	-5.21
$\text{UO}_2^{2+} + 2\text{H}_2\text{O} = \text{UO}_2(\text{OH})_2^0 + 2\text{H}^+$	-12.0
$\text{UO}_2^{2+} + 3\text{H}_2\text{O} = \text{UO}_2(\text{OH})_3^- + 3\text{H}^+$	-19.22
$2\text{UO}_2^{2+} + 3\text{H}_2\text{O} + \text{CO}_3^{2-} = (\text{UO}_2)_2\text{CO}_3(\text{OH})_3^- + 3\text{H}^+$	-0.890

Table 4

A comparison of different models for UO_2^{2+} adsorption onto *S. putrefaciens*

W_{sos}/df values are sums of squares of residuals computed by FITEQL. W_{sos}/df values are not directly comparable among experiments, but may be used to compare different models of a single data set.

Single complex	1.72 g bacteria/1 10 μM U ($I = 0.1$)		17.2 g bacteria/1 10 μM U ($I = 0.1$)		1.72 g bacteria/1 10 μM U ($I = 0.02$)	
	log K	W_{sos}/df	log K	W_{sos}/df	log K	W_{sos}/df
> COO– UO_2^+	2.84	0.276	4.96	0.773	3.42	1.01
> COO– UO_2OH	–1.95	5.60	–1.39	2.34	–3.03	7.83
> COO– UO_2CO_3^-	10.1	14.6	14.3	7.64	10.6	12.1
> COOH– UO_2^{++}	10.1	3.60	12.5	0.786	11.3	7.11
> COOH– UO_2CO_3	17.4	4.51	20.2	0.250	18.4	2.90
> COOH– $\text{UO}_2(\text{OH})_2$	–1.95	5.60	–1.39	2.34	–3.03	7.83
> COO– UO_2 –COO <	2.42	0.659	4.49	0.203	3.23	0.540
> PO_4 – UO_2^+	2.55	2.44	2.30	0.341	3.15	1.19
> PO_4 – UO_2OH	–2.18	9.60	–2.85	6.51	2.39	0.182
> PO_4 – UO_2CO_3^-	11.6	15.7	10.6	18.0	9.80	17.7
> PO_4H – UO_2^{++}	8.36	2.29	10.0	0.786	9.64	6.78
> PO_4H – UO_2CO_3	18.8	5.63	18.9	1.36	17.0	9.56
> PO_4H – $\text{UO}_2(\text{OH})_2$	–2.18	9.60	–2.85	6.51	2.39	0.182
> PO_4 – UO_2 – PO_4 <	4.05	4.31	1.40	2.99	4.37	6.64
> OH– UO_2^{++}	11.7	3.93	12.5	0.127	12.2	3.06
> OH– UO_2OH^+	4.80	16.8	7.97	13.1	4.74	16.4
> OH– UO_2CO_3	19.2	21.1	20.1	23.6	18.9	21.0
> OH– $\text{UO}_2(\text{OH})_2$	3.77	35.1	7.64	10.8	5.27	14.0
> OH_2 – UO_2CO_3^+	25.3	13.0	27.9	3.32	25.7	10.8
> OH_2 – $\text{UO}_2(\text{OH})_2^+$	4.80	16.8	10.0	10.8	4.74	16.4
> OH– UO_2CO_3 –OH <	24.3	39.0	39.7	5.28	36.1	14.1
> OH_2 – $\text{UO}_2(\text{OH})_3$	3.77	35.1	7.64	10.8	5.27	14.0
Two complexes	log K	W_{sos}/df	log K	W_{sos}/df	log K	W_{sos}/df
> COO– UO_2^+	2.64	0.144	No Convergence		2.84	0.219
> PO_4 – UO_2^+	1.58				2.52	
> COO– UO_2^+	2.64	0.150	No Convergence		2.90	0.192
> OH– UO_2^{++}	10.8				11.5	
> COO– UO_2^+	2.68	0.173	2.49	0.070	2.96	0.249
> PO_4H – $\text{UO}_2(\text{OH})_2$	–5.51		–4.72		–4.85	
> COO– UO_2^+	2.64	0.130	2.49	0.183	2.91	0.241
> PO_4H – UO_2CO_3	15.2		16.5		16.1	
> COO– UO_2^+	2.84	0.255	4.95	0.798	3.39	0.993
> OH_2 – $\text{UO}_2(\text{OH})_3$	–4.91		–4.83		–4.32	
> COO– UO_2^+	2.68	0.160	2.51	0.081	2.98	0.239
> OH_2 – $\text{UO}_2(\text{CO}_3)_2^-$	31.1		33.0		31.7	

Relatively close fits to the experimental data are obtained for models involving > COO– UO_2^+ and a second surface complex that is electrically neutral, such as > PO_4H – $\text{UO}_2(\text{OH})_2$, > PO_4H – UO_2CO_3 or > OH_2 – $\text{UO}_2(\text{OH})_3$. A model employing > OH_2 – $\text{UO}_2(\text{OH})_3$ and > COO– UO_2^+ provides a fairly good fit to each experimental data set, but the different estimated log K values for > COO– UO_2^+ forma-

tion range over two orders of magnitude; from 2.84 to 4.95. Because of this broad spread in values, an average log K for > COO– UO_2^+ formation (for this two-reaction scheme) does not predict the speciation of U in any of the individual experiments. A moderately good fit is obtained if the negatively charged complex > OH_2 – $\text{UO}_2(\text{CO}_3)_2^-$ is used along with > COO– UO_2^+ , however the different log K values

obtained for the reaction forming $>OH_2-UiO_2-(CO_3)_2^-$ also display a divergence of about two orders of magnitude, from 31.1 to 33.0.

Models with $>PO_4H-UiO_2(OH)_2$ or $>PO_4H-UiO_2CO_3$ as a second complex show close correspondence with the experimental data and converge on similar results for log K values. A model of uranyl sorption employing the complexes $>PO_4H-UiO_2(OH)_2$ and $>COO-UiO_2^+$ yields a narrow range in log K values for each complex; 0.79 log units and 0.28 log units, respectively. A model employing the complexes $>PO_4H-UiO_2CO_3$ and $>COO-UiO_2^+$ yields a slightly wider range of log K values; 1.3 and 0.42 log units, respectively. Both of these two-complex models provide better fits to the experimental data than a single bidentate uranyl-carboxyl surface complex.

7. Discussion

7.1. Acid–base properties of the cell envelope

Optimal model fits to the titration data indicate that the outer aspect of the outer cell membrane of *S. putrefaciens*, grown under the conditions outlined above, can be reasonably approximated as a surface having two major types of negatively ionizing surface sites ($>XH$ and $>ZH$) and one type of positively ionizing site ($>YH$). The optimal value of pK_a for the $>ZH$ site is 5.16 ± 0.04 and its computed site density is $31.7 \mu\text{mol sites/g bacteria}$ ($0.35 \pm 0.02 \text{ sites/nm}^2$, assuming an SSA of $55 \text{ m}^2/\text{g}$), where reported uncertainties are 1σ standard deviations of model results for three different titrations. For the $>XH$ site the average pK_a is 7.22 ± 0.15 and the average site density is $9.85 \mu\text{mol sites/g bacteria}$ ($0.11 \pm 0.007 \text{ sites/nm}^2$). The base site $>YH$ is estimated to have a pK_a value of 10.04 ± 0.67 and a site density of $38.0 \mu\text{mol sites/g bacteria}$ ($0.42 \pm 0.008 \text{ sites/nm}^2$). Site densities are provided in terms of moles of sites per gram of bacteria assuming 10^{12} bacteria/g (DiChristina, 1989), and also in terms of sites/ nm^2 assuming that the bacterial surface can be approximated as a single layer. Because of the complex and layered structure of the outer membrane it is probably not realistic to assume that all ionizable functional groups on the

bacteria occupy a single surface layer analogous to a mineral surface. However, a value of site concentration per unit surface area may be useful as a benchmark value in comparing the results of one study with another. Both expressions of site concentration ($\mu\text{mol sites/g}$ and sites/nm^2) are based, however, on assumptions relating cell mass to surface area.

Alternatively, site concentrations may be expressed in terms of the number of sites per bacterium. This approach is advantageous in that the only additional source of significant error beyond that associated with the model calculation itself derives from the error on cell density. Cell densities were measured in this study using an AODC method (Lovley and Phillips, 1988) that in this study typically yielded errors of $\sim 10\%$ or lower on cell counts of replicate cell-suspension aliquots. Thus, errors on site densities are realistically on the order of $\sim 10\%$ in Megasites/bacterium. Site concentrations in these units were estimated to be: $>XH = 5.93 \pm 0.6$, $>YH = 22.9 \pm 2$, and $>ZH = 19.1 \pm 2$ Megasites/bacterium.

Model results at different cell densities are similar, indicating a robust fit to the experimental data. Statistical uncertainties on pK_a values and site densities are below 7% despite the small number ($N = 3$) of titration data sets that were compared. Uncertainties on pK_a values are likely to be independent of absolute errors on bacterial density. This is because pK_a values are determined largely by the shapes of titration curves and not the absolute values of $[H^+]_{\text{exchanged}}$, which depend on the absolute concentrations of buffering sites. Values of pK_a are determined largely by the pH dependence of $\delta\text{pH}/\delta V$ during a titration. This is illustrated in Fig. 1, which shows that titration curves “shallow” with decreasing bacterial density, while the overall shapes of the curves remain essentially constant regardless of the number of bacteria present in solution. It is therefore reasonable to assign uncertainties to pK_a values that equal errors associated with the model optimization and the titration procedure itself.

It is not possible to uniquely identify the compositions of functional groups by their pK_a values alone. Unequivocal identification of the types of functional groups responsible for acid–base buffering must be provided by other techniques that yield compositional data. In particular, spectroscopic techniques

such as Fourier transform infrared spectroscopy (FTIR) of adsorbed complexes on cell surfaces, or gas/liquid chromatography of cell membrane extracts could potentially identify functional groups responsible for pH-buffering and metal sorption. Investigations of this kind are beyond the intended scope of this current work, but would be useful in further elucidating the coordination chemistry of *S. putrefaciens* cell envelopes. Constrained pK_a values may, however, be used to suggest or exclude possible functionalities.

The optimal pK_a value for the >XH site is 7.22 ± 0.15 . This is close to the value for the second dissociation constant for phosphoric acid ($pK_{a_2} = 7.20$) and may therefore represent deprotonation of a surface phosphoryl group associated with cell membrane phospholipids or phosphorylated polysaccharides. Phosphate groups are linked to glucosamine in the lipid A region of the outer cell membrane, and are also found in association with heptose units of the core polysaccharide region of LPS (Madigan et al., 2000). The >XH site is unlikely to be a carboxyl group. pK_a values of amino acid α -carboxyl groups range from 1.80 (histidine) to 2.35 (glycine, alanine), while the γ -carboxyl side chain of glutamic acid is 4.07 (Dawson et al., 1986). Carboxyl side chains of proteins (Creighton, 1997) can display shifts in pK_a values of several log units due to conformational and hydrogen-bonding effects, however a value of ~ 7 is probably too basic to be attributed to proteinic carboxyl side-groups. Consequently, we propose that the >XH site represents phosphoryl (>PO₄H) groups associated with the outer membrane phospholipid and LPS components. Fein et al. (1997) reported a similar model estimate of pK_a (6.9) for surface phosphoryl groups on *B. subtilis*.

The >ZH site is more likely to represent carboxyl groups found in association with the outer cell membrane. Its pK_a value of 5.16 ± 0.04 is similar to that of the glutamic acid γ -carboxyl moiety and is easily within the range of pK_a values for amino carboxyl side-chains on proteins. A second source of carboxyl groups on the bacterial surface may be found in the LPS layer, however this region on *S. putrefaciens* is relatively poor in free carboxyl groups. Most carboxyl groups exhibited by fatty acids in the lipid A region are bound in ester link-

ages to other fatty acids. Free carboxyl groups are only found within the KDO component of the core polysaccharide complex, where each LPS strand is linked to lipid A by a bridging KDO unit that possesses one carboxyl group per *ortho*-KDO molecule. This source of carboxyl groups is essentially ubiquitous on the cell surface because the KDO component links LPS to the outer membrane. The density of >XH sites on the bacterial surface is estimated to be ~ 0.35 sites/nm². This value compares favorably with an approximate separation of 1.4 nm between LPS polysaccharide chains (Moule and Wilkinson, 1989), resulting in a maximum LPS density of ~ 0.51 strands/nm². KDO of Gram negative bacteria can occur as single bridging units or can possess non-bridging KDO side-chains attached to the core KDO unit. Bridging KDO of *S. putrefaciens* lacks additional side-chains, suggesting that a maximum carboxyl site density of ~ 0.51 sites/nm² is expected on structural grounds. Regressions of titration data by Fein et al. (1997) for *B. subtilis* yield a best-fit pK_a of 4.82, which those authors also attribute to surface carboxyl groups.

The modeled base site >YH is probably an amine group, based on its pK_a value of 10.0 ± 0.67 and its predicted ability to acquire a positive electrostatic charge. Its pK_a value corresponds closely with the range of pK_a values for α -amino groups on free amino acids (Dawson et al., 1986), thiol side-chains of proteins (Creighton, 1997), and phenolic hydroxyl groups. If >YH is predominantly amine in composition this site could occur within the LPS or on wall proteins. LPS components that exhibit amine groups include glucosamine (average 6.8% by weight normalized in LPS: Moule and Wilkinson, 1989), D-galactosamine (average 3.2%) and 3-amino-3,6-dideoxyglucose (average 1.0%). Wall proteins and porins will contribute significantly to the abundance of ionizable amine groups, but the extent of this contribution is not easily quantifiable within the scope of the present study. Fig. 6 illustrates the estimated surface speciation of *S. putrefaciens* as a function of pH and in terms of percent species referenced to the most abundant (amine) site.

The overall pH-buffering capacity of *S. putrefaciens* appears to be less than that of Gram positive bacteria of similar size. Daughney et al. (1998) and Fein et al. (1997) found that different strains of the

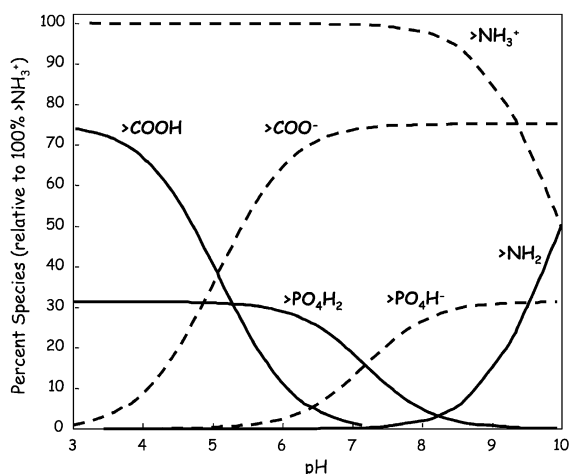


Fig. 6. Estimated speciation profile of the *S. putrefaciens* surface according to a three-site depiction, calculated using the constant capacitance model. Values are plotted as a function of pH versus percent species. Percentile abundances are referenced to the predicted amine site concentration as 100%.

Gram positive aerobic *Bacillus* possess carboxyl site densities in the range ~ 89 – $120 \mu\text{mol sites/g}$ bacteria, compared with our estimate for *S. putrefaciens* of $\sim 32 \mu\text{mol sites/g}$ bacteria. Our estimate of the concentration of ionizable phosphoryl groups on the *S. putrefaciens* surface is similarly lower ($\sim 9.9 \mu\text{mol sites/g}$ bacteria) than that of *Bacillus* sp. (~ 44 – $83 \mu\text{mol/g}$ bacteria) according to Daughney et al. (1998) and Fein et al. (1997). Furthermore, our study indicates a strong amino-group component to pH buffering that is previously unreported for *Bacillus* bacteria. In contrast, Fein et al. (1997) and Daughney et al. (1998) found that hydroxyl groups strongly buffered pH in the basic region, contributing to the overall negative charge of the bacterial surface. Unlike *Bacillus* sp., *S. putrefaciens* exhibits a net positive charge under acidic pH conditions. Fein et al. (1997) and Daughney et al. (1998) found that the surfaces of *B. subtilis* and *B. licheniformis* are both neutrally charged at pH values below ~ 3.8 and negatively charged at more basic pH values. These different results probably stem from the differing structures and compositions of Gram negative and positive cell membranes. The Gram positive membrane is surrounded by PG that is predominantly anionic in nature, while the Gram negative outer membrane exhibits a mixture of LPS and protein that

is likely to contain a higher complement of amine groups. Under optimal pH conditions for growth (pH = 7), *S. putrefaciens* will exhibit a neutral to slightly positive net surface charge, whereas *Bacillus* sp. will exhibit a net negative charge under similar conditions. It is interesting to note that at a pH of 7–8 the surface of *S. putrefaciens* will carry a net neutral charge while the surfaces of most Fe-oxide minerals, upon which this bacteria will typically respire under anaerobic conditions, will also carry a net neutral charge (Stumm and Morgan, 1996). The electrostatics of both cell and mineral would, in this case, favor the hydrophobic or Van der Waals adhesion of each surface onto the other. Further studies are necessary to investigate the likely dependence of Fe(III)-oxide reduction rates on *S. putrefaciens*–mineral attachment.

7.2. Uranium sorption at the cell envelope

Sorption experiments using *S. putrefaciens* reveal a pH and substrate-concentration dependence on U sorption that is similar to that exhibited by mineral surfaces (Ho and Doern, 1985; Hsi and Langmuir, 1985; Ho and Miller, 1985, 1986; Payne and Waite, 1991; Waite et al., 1994; Gabriel et al., 1998; Liger et al., 1999; Lenhart and Honeyman, 1999), other bacteria (Friis and Myers-Keith, 1986; Cotoras et al., 1992a,b; Fowle et al., 2000), and lichens (Haas et al., 1998). Minimal uptake of U was observed in this study at pH values below ~ 2 or above ~ 9 , although significant sorption was measured in the pH interval 3–8, depending on bacteria:U concentration ratio. Only a weak dependence of U sorption on ionic strength was observed over the range $I = 0.02$ – 0.1 , and the manner of this dependence was consistent with expectations based on ion-interaction theory.

The experimental data could be modeled as a result of U adsorption by the bacteria onto predicted surface carboxyl and phosphoryl groups. Surface-complexation models involving only one type of sorbing U complex do not closely reproduce the experimental data, but model fits are improved by the inclusion of a second, separate surface complex. U sorption under acidic pH conditions was best accounted for by the formation of a monodentate uranyl–carboxyl surface complex ($> \text{COO}-\text{UO}_2^+$),

while U sorption under weakly acid to near-neutral pH conditions was best explained by a neutrally charged surface complex on the phosphoryl site. The experimental data could be best approximated using either $>PO_4H-UO_2(OH)_2$ or $>PO_4H-UO_2CO_3$ as this second complex, with $>PO_4H-UO_2(OH)_2$ providing slightly better reproducibility in log K values under differing experimental conditions.

The inclusion of $>COO-UO_2^+$ in numerical calculations yields a remarkably similar log K value for this complex in a wide variety of speciation models. The robustness of this result demonstrates that U sorption in the acidic pH range can be largely accounted for with a one-site surface complexation model. Up to a pH of ~ 5 under experimental conditions the aquo species UO_2^{2+} is predicted to dominate U aqueous speciation. Under these conditions the predicted carboxyl site becomes increasingly negatively charged with increasing pH in the range 3–6. It is thus geochemically reasonable to postulate the formation of a surface complex between the negatively charged carboxyl site and the positively charged aquo-uranyl ion in the pH range 2–6. However, retention of U by the bacterial surface at a pH > 6 , as observed experimentally, requires the formation of a second surface complex.

The requirement of a second surface complex is best fulfilled by using either $>PO_4H-UO_2(OH)_2$ or $>PO_4H-UO_2CO_3$ to account for U sorption at pH

values higher than ~ 5 . These two surface complexes are similar, differing only in the types of uranyl complexes that sorb onto the phosphoryl site. The aqueous complexes $UO_2(OH)_2$ and UO_2CO_3 are predicted to dominate U aqueous speciation in the near-neutral pH range under atmospheric CO_2 concentrations. It is therefore reasonable to expect that these species may tend to sorb onto the predicted phosphoryl site, which will be neutrally charged at pH values below ~ 7.2 . Neutral aqueous species would probably sorb weakly through Van der Waals attraction to the neutral protonated $>PO_4H$ site. Use of the $>PO_4H-UO_2(OH)_2$ species provides slightly smaller statistical uncertainties on estimated log K values than does use of $>PO_4H-UO_2CO_3$. For this reason, and because we estimate the aqueous speciation of U under our experimental conditions to be dominated by $UO_2(OH)_2$ over UO_2CO_3 by approximately a factor of two in the pH range of interest, we opt for $>PO_4H-UO_2(OH)_2$ as a better model for U sorption in the near-neutral pH range. Fig. 7 illustrates calculated adsorption curves for this two-complex model, compared with experimental U uptake data.

Our results are similar, in terms of adsorption stoichiometries, to those obtained by Fowle et al. (2000) for U sorption onto *B. subtilis*. In their study those authors find that an optimal model of U sorption is obtained using a two-reaction scheme where

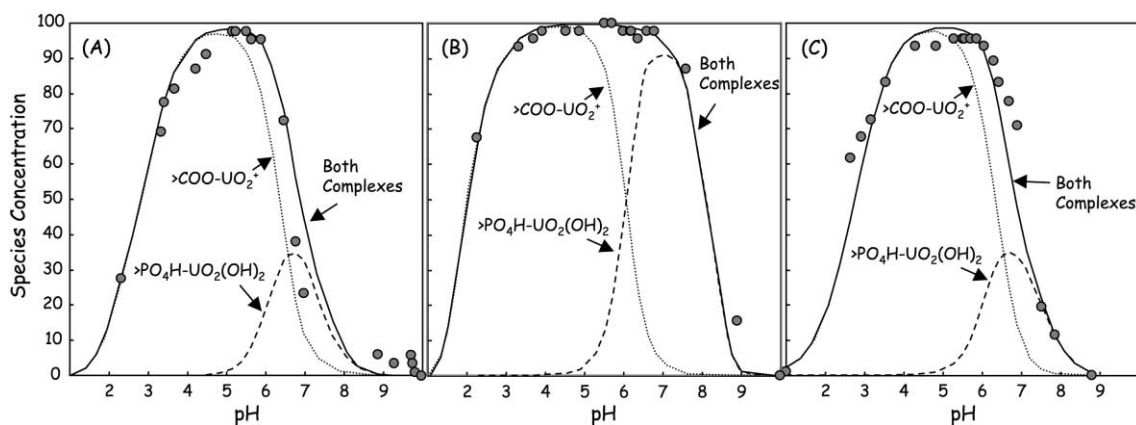


Fig. 7. Experimental U sorption data and calculated speciation curves for an optimal U(VI)–*S. putrefaciens* sorption model involving two separate surface complexes. Initial aqueous U concentration was $10 \mu M$ for all experiments. Experimental conditions: (A) 1.72 g bacteria/l, $I = 0.1 M$ NaCl; (B) 17.2 g/l, $0.1 M$ NaCl; (C) 1.72 g/l, $0.02 M$ NaCl.

aquo uranyl sorbs onto (1) a deprotonated surface carboxyl site and (2) a protonated neutral phosphoryl site. Our log K value for $>COO-UO_2^+$ complexation (average ~ 2.71) differs from that of Fowle et al. (2000) (5.4 ± 0.2) by nearly three orders of magnitude, despite both bacteria having similar surface-carboxyl pK_a values (*S. putrefaciens* our study = 5.2, *B. subtilis* = 4.8, *B. licheniformis* = 5.2), and having specific site densities that are similar within a factor of three (Fein et al., 1997; Daughney et al., 1998; Fowle et al., 2000). These different results for *S. putrefaciens* and *B. subtilis* support a hypothesis that different types of bacteria can possess significantly different geochemical properties, and therefore that estimating the speciation of aqueous ions in the subsurface probably cannot be accomplished by including one standard bacterial component in chemical speciation and reactive transport models.

S. putrefaciens, unlike Gram positive forms such as *Bacillus*, appears to exhibit a positively charged surface at pH values lower than ~ 7.5 . This feature has important implications for the coordination of metal ions to the bacterial surface under acidic pH conditions. Surface complexation theory predicts that net positive surfaces will tend to repel cations electrostatically, but our experiments demonstrate strong U sorption at pH values as low as ~ 2 . One potential explanation for this observation may relate to the distribution of surface charge. If most positive charges on *S. putrefaciens* are localized, for example on wall-mounted proteins, regions of the cell surface lacking those proteins but possessing active carboxyl or phosphoryl groups would still display a net negative charge. Alternately, both positive and negative charges could occur on different proteins, or on the same protein at locations distantly separated from each other. Our estimated site densities for amine, carboxyl and phosphoryl functionalities are 0.1–0.4 sites/nm², yielding an average intersite distance of 2.5–10 nm. A separation of greater than ~ 1 nm would be greater than the thickness of the electrical double layer, indicating that each point charge on the bacterial surface could interact quasi-independently with ions in the overlying solution. Additional work is required to further constrain the location of charge-bearing functionalities on the *S. putrefaciens* surface, and to evaluate their spatial distribution as a function of pH and ion coordination.

8. Concluding remarks

The results of this study demonstrate that U sorption onto Gram negative MRB, using *S. putrefaciens* as a model organism, is significant at environmentally reasonable cell densities (10^8 – 10^{10} cells/ml), U concentrations (10 μ M), and pH values (3–8). This study provides site-specific stability constants for U sorption onto *S. putrefaciens* and values constraining the surface properties of this bacterium as a function of pH. The specified values are best used in the context of a surface complexation approach to estimate the speciation of U in systems comprising water, minerals and bacteria. Our findings suggest that anaerobic MRB could play a significant role in the biogeochemical cycling and transport of redox-sensitive radionuclides, including U but also potentially Pu, Np, Am and Tc. Because U(VI) reduction can lead to the formation of insoluble U(IV) phases such as uraninite (UO₂), MRB could also prove useful in retarding the migration of radionuclides in anoxic ground waters.

The relationship between sorption and respiration is not addressed in this study, but is an important question. Do *S. putrefaciens* and similar MRB that can grow on U(VI) require sorption as a prerequisite for growth? It is likely that U(VI) is either reduced directly on the outer aspect of the cell membrane or is brought into the periplasm where it is reduced and then insoluble U(IV) secreted from the cell. In either case, surface complexation may govern the rate of growth on this TEA. Liger et al. (1999) found that the rate of abiotic U(VI) reduction by Fe(II) where both ions are sorbed onto hematite depends strongly on the surface speciation of U and Fe. It is likely that speciation also governs the bioavailability of metals to MRB capable of their reduction. Further studies to evaluate this hypothesis would be useful in revealing further the linkage between chemical thermodynamics and the biogeochemical cycling of U, Fe and other metallic elements in the geologic environment.

Acknowledgements

This work was supported in part by the Environmental Protection Agency, the Nelson and Bennie Abell Professorship in Biology at Georgia Tech, and

by Western Michigan University (WMU). The authors benefited greatly from many helpful discussions with Carla Koretsky, Philippe van Cappellen, Charlie Moore, Carolyn Haller, Patricia Sobbecky, Suvasis Dixit, and Thilo Behrends. This is contribution #1 of the Microbial Aqueous Geochemistry, Biogeochemistry and Thermodynamics (MAGBAT) laboratory at WMU.

References

- Barker, W.W., Haas, J.R., Suzuki, Y., Banfield, J.F., 1998. U-phosphate biomineralization as a mechanism of U fixation by lichen. *Geol. Soc. Am.* 30 (6), 205, Abstracts with Programs.
- Barns, S.M., Nierzwicki-Bauer, S., 1997. Microbial diversity in modern subsurface, ocean, surface environments. In: Banfield, J.F., Nealson, K.H. (Eds.), *Geomicrobiology: Interactions between Microbes and Minerals*. Reviews in Mineralogy, vol. 35, Mineralogical Society of America, pp. 35–80.
- Beveridge, T.J., Fyfe, W.S., 1985. Metal fixation by bacterial cell walls. *Can. J. Earth Sci.* 22, 1892–1898.
- Beveridge, T.J., Koval, S.F., 1981. Binding of metal ions to cell envelopes of *Escherichia coli* K-12. *Appl. Environ. Microbiol.* 42, 325–335.
- Beveridge, T.J., Forsberg, C.W., Doyle, R.J., 1982. Major sites of metal binding in *Bacillus licheniformis* walls. *J. Bacteriol.* 150, 1438–1448.
- Birdsell, D.C., Cota-Robles, E.H., 1967. Production and ultrastructure of lysozyme and ethylenediaminetetraacetate-lysozyme spheroplasts of *Escherichia coli*. *J. Bacteriol.* 93, 427–437.
- Bruno, J., De Pablo, J., Duro, L., Figuerola, E., 1995. Experimental study and modeling of the U(VI)–Fe(OH)₃ surface precipitation/coprecipitation equilibria. *Geochim. Cosmochim. Acta*, 59, 4113–4123.
- Costerton, J.W., 1970. The structure and function of the cell envelope of Gram negative bacteria. *Rev. Can. Biol.* 29, 299–316.
- Costerton, J.W., Forsberg, C., Matula, T.I., Buckmire, F.L.A., Macleod, R.A., 1967. Nutrition and metabolism of marine bacteria: XVI. Formation of protoplasts, spheroplasts, and related forms from a Gram negative marine bacterium. *J. Bacteriol.* 94, 1764–1777.
- Creighton, T.E., 1997. *Proteins: Structures and Molecular Properties*. Freeman, New York.
- Cotoras, D., Millar, M., Viedma, P., Pimentel, J., Mestre, A., 1992a. Biosorption of metal-ions by *Azotobacter vinelandii*. *World J. Microbiol. Biotechnol.* 8 (3), 319–323.
- Cotoras, D., Viedma, P., Cifuentes, L., Mestre, A., 1992b. Sorption of metal ions by whole cells of *Bacillus* and *Micrococcus*. *Environ. Technol.* 13 (6), 551–559.
- Daughney, C.J., Fein, J.B., Yee, N., 1998. A comparison of the thermodynamics of metal adsorption onto two common bacteria. *Chem. Geol.* 144, 161–176.
- Davis, J.A., Kent, D.B., 1990. Surface complexation modeling in aqueous geochemistry. In: Hochella, J.M.F., White, A.F. (Eds.), 1990. *Mineral–Water Interface Geochemistry*, vol. 23, Mineralogical Society of America, pp. 177–260.
- Dawson, R.M.C., Elliott, D.C., Jones, K.M., 1986. *Data for Biochemical Research*. Oxford Science Publications.
- DiChristina, T.J., 1989. Dissimilative Fe(III) reduction by *Alteromonas putrefaciens* strain 200. PhD Dissertation, California Institute of Technology, Pasadena, CA.
- DiChristina, T.J., DeLong, E.F., 1994. Isolation of anaerobic respiratory mutants of *Shewanella putrefaciens* and genetic analysis of mutants deficient in anaerobic growth on Fe³⁺. *J. Bacteriol.* 176, 1468–1474.
- Fein, J.B., Delea, D., 1999. Experimental study of the effect of EDTA on Cd adsorption by *Bacillus subtilis*: a test of the chemical equilibrium approach. *Chem. Geol.* 161, 375–383.
- Fein, J.B., Daughney, C.J., Yee, N., Davis, T.A., 1997. A chemical equilibrium model for metal adsorption onto bacterial surfaces. *Geochim. Cosmochim. Acta* 61, 3319–3328.
- Friis, N., Myers-Keith, P., 1986. Biosorption of uranium and lead by *Streptomyces longwoodensis*. *Biotechnol. Bioeng.* 28 (1), 21–28.
- Fortin, D., Ferris, F.G., Beveridge, T.J., 1997. Surface-mediated mineral development by bacteria. In: Banfield, J.F., Nealson, K.H. (Eds.), *Geomicrobiology: Interactions Between Microbes and Minerals*. Reviews in Mineralogy, vol. 35. Mineralogical Society of America.
- Fowle, D.A., Fein, J.B., 1999. Competitive adsorption of metal cations onto two Gram positive bacteria: testing the chemical equilibrium model. *Geochim. Cosmochim. Acta* 63, 3059–3067.
- Fowle, D.A., Fein, J.B., Martin, A.M., 2000. Experimental study of uranyl adsorption onto *Bacillus subtilis*. *Environ. Sci. Technol.* 34, 3737–3741.
- Gabriel, U., Gaudet, J.P., Spadini, L., Charlet, L., 1998. Reactive transport of uranyl in a goethite column: an experimental and modelling study. *Chem. Geol.* 151, 107–128.
- Grenthe, I., Fuger, J., Konings, R.J.M., Lemire, R.J., Muller, A.B., Nguyen-Trung, C., Wanner, H., 1992. *Chemical Thermodynamics*. Vol. 1: *Chemical Thermodynamics of Uranium*. North-Holland, Amsterdam.
- Haas, J.R., Bailey, E.H., Purvis, O.W., 1998. Bioaccumulation of metals by lichens: uptake of aqueous uranium by *Peltigera membranacea* as a function of time and pH. *American Mineralogist* 83, 1494–1502 (11–12, Part 2).
- Hayes, K.F., Leckie, J.O., 1987. Modeling ionic strength effects on cation adsorption at hydrous-oxide/solution interfaces. *J. Coll. Int. Sci.* 115, 564–572.
- He, L.M., Tebo, B.M., 1998. Surface charge properties of and Cu(II) adsorption by spores of the marine *Bacillus* sp. strain SG-1. *Appl. Environ. Microbiol.* 64, 1123–1129.
- Ho, C.J., Doern, D.C., 1985. The adsorption of uranyl species on a hematite sol. *Can. J. Chem.* 63, 1100–1104.
- Ho, C.J., Miller, N.H., 1985. Effect of humic acid on uranium uptake by hematite particles. *J. Coll. Int. Sci.* 106, 281–288.
- Ho, C.J., Miller, N.H., 1986. Adsorption of uranyl species from bicarbonate solution onto hematite particles. *J. Coll. Int. Sci.* 110, 165–171.

- Hodgkiss, W., Shewan, J.M., 1968. Problems and modern principles in the taxonomy of marine bacteria. In: Droop, M.R., Wood, E.J.F. (Eds.), *Advances in Microbiology of the Sea*. Academic Press, New York, pp. 127–166.
- Hsi, C.D., Langmuir, D., 1985. Adsorption of uranyl onto ferric oxyhydroxides: application of the surface complexation site-binding model. *Geochim. Cosmochim. Acta* 49, 1931–1941.
- Kohler, M., Curtis, G.P., Kent, D.B., Davis, J.A., 1996. Experimental investigation and modeling of uranium(VI) transport under variable chemical conditions. *Water Resour. Res.* 32, 3539–3551.
- Langley, S., Beveridge, T.J., 1999. Effect of *O*-side-chain-lipopolysaccharide chemistry on metal binding. *Appl. Environ. Microbiol.* 65, 489–498.
- Lee, J.V., 1979. *Alteromonas (Pseudomonas) putrefaciens*. In: Russell, A.D., Fuller, R. (Eds.), *Cold Tolerant Microbes in Spoilage and the Environment*. Academic Press, London, pp. 59–65.
- Lenhart, J.J., Honeyman, B.D., 1999. Uranium(VI) sorption to hematite in the presence of humic acid. *Geochim. Cosmochim. Acta* 63, 2891–2901.
- Liger, E., Charlet, L., Van Cappellen, P., 1999. Surface catalysis of Uranium (VI) reduction by Iron (II). *Geochim. Cosmochim. Acta* 63, 2939–2955.
- Lloyd, J.R., Nolting, H.-F., Solé, V.A., Bosecker, K., Macaskie, L.E., 1998. Technetium reduction and precipitation by sulfate-reducing bacteria. *Geomicrobiol. J.* 15, 45–58.
- Lloyd, J.R., Ridley, J., Khizniak, T., Lyalikova, N., Macaskie, L.E., 1999. Reduction of technetium by *Desulfovibrio desulfuricans*: biocatalyst characterization and use in a flow-through bioreactor. *Appl. Environ. Microbiol.* 65, 2691–2696.
- Lovley, D.R., 1991. Dissimilatory Fe(III) and Mn(IV) reduction. *Microbiol. Rev.* 55, 259–287.
- Lovley, D.R., Phillips, E.J.P., 1988. Novel mode of microbial energy metabolism: organic carbon oxidation coupled to dissimilatory reduction of iron or manganese. *Appl. Environ. Microbiol.* 54, 1472–1480.
- Lovley, D.R., Phillips, E.J.P., Gorby, Y.A., Landa, E.R., 1991. Microbial reduction of uranium. *Nature* 350, 413–416.
- Lovley, D.R., Giovannoni, S.J., White, D.C., Champine, E.J., Phillips, E.J.P., Gorby, Y.A., Goodwin, S., 1993. *Geobacter metallireducens* gen. nov. sp. nov., a microorganism capable of coupling the complete oxidation of organic compounds to the reduction of iron and other metals. *Arch. Microbiol.* 159, 336–344.
- MacDonell, M.T., Colwell, R.R., 1985. Phylogeny of the vibriaceae, and recommendation for two new genera, *Listonella* and *Shewanella*. *Syst. Appl. Microbiol.* 6, 171–182.
- Madigan, M.T., Martinko, J.M., Parker, J., 2000. *Brock Biology of Microorganisms*. Prentice Hall, New Jersey.
- Moule, A.L., Wilkinson, S.G., 1989. Composition of lipopolysaccharides from *Alteromonas putrefaciens (Shewanella putrefaciens)*. *J. Gen. Microbiol.* 135, 163–173.
- Moulin, V., Ouzounian, G., 1992. Role of colloids and humic substances in the transport of radioelements through the geosphere. *Appl. Geochem.* 1, 179–186 (suppl.).
- Nealson, K.H., Saffarini, D., 1994. Iron and Manganese in anaerobic respiration: environmental significance, physiology, and regulation. *Annu. Rev. Microbiol.* 48, 311–343.
- Nealson, K.H., Stahl, D.A., 1997. Microorganisms and biogeochemical cycles: what can we learn from layered microbial communities? In: Banfield, J.F., Nealson, K.H. (Eds.), *Geomicrobiology: Interactions Between Microbes and Minerals*. Reviews in Mineralogy, vol. 35. Mineralogical Society of America.
- Obuekwe, C.O., Westlake, D.W.S., Cook, F.D., 1981. Effect of nitrate on reduction of ferric iron by a bacterium isolated from crude oil. *Can. J. Microbiol.* 27, 692–697.
- Payne, T.E., Waite, T.D., 1991. Surface complexation modelling of uranium sorption data obtained by isotope exchange techniques. *Radiochim. Acta* 52/53, 487–493.
- Prapaipong, P., Shock, E.L., Koretsky, C.M., 1999. Metal–organic complexes in geochemical processes: temperature dependence of the standard thermodynamic properties of aqueous complexes between metal cations and dicarboxylate ligands. *Geochim. Cosmochim. Acta* 63 (17), 2547–2577.
- Prikryl, J.D., Pabalan, R.T., Turner, D.R., Leslie, B.W., 1994. Uranium sorption on α -alumina: effects of pH and surface area/solution volume ratio. *Radiochim. Acta* 66/67, 291–296.
- Read, D., Bennett, D.G., Hooker, P.J., Ivanovich, M., Longworth, G., Milodowski, A.E., Noy, D.J., 1993. The migration of uranium into peat-rich soils at Broubster, Caithness, Scotland, UK. *J. Cont. Hydrol.* 13, 291–308.
- Rusin, P.A., Quintana, L., Brainard, J.R., Strietelmeier, B.A., Tait, C.D., Ekberg, S.A., Palmer, P.D., Newton, T.W., Clark, D.L., 1994. Solubilization of plutonium hydrous oxide by iron-reducing bacteria. *Environ. Sci. Technol.* 28, 1686–1690.
- Sagert, N.H., Ho, C.H., Miller, N.H., 1989. The adsorption of uranium(VI) onto a magnetite soil. *J. Coll. Int. Sci.* 130, 283–287.
- Sahai, N., Sverjensky, D.A., 1997. Solvation and electrostatic model for specific electrolyte adsorption. *Geochim. Cosmochim. Acta* 61, 2827–2848.
- Schultze-Lam, S., Urrutia-Mera, M., Beveridge, T.J., 1995. Metal and silicate sorption and subsequent mineral formation on bacterial surfaces: subsurface implications. In: Allen, H.E. (Ed.), *Metal Contaminated Aquatic Sediments*. Ann Arbor Press, Ann Arbor, pp. 111–147.
- Sheppard, M.A., Thibault, D.H., 1992. Desorption and extraction of selected heavy metals from soils. *Soil Sci. Soc. Am. J.* 56, 415–423.
- Shock, E.L., Koretsky, C.M., 1993. Metal–organic complexes in geochemical processes: calculation of standard partial molal thermodynamic properties of aqueous acetate complexes at high pressures and temperatures. *Geochim. Cosmochim. Acta* 57, 4899–4922.
- Shock, E.L., Koretsky, C.M., 1995. Metal–organic complexes in geochemical processes: estimation of standard partial molal thermodynamic properties of aqueous complexes between metal cations and monovalent organic acid ligands at high pressures and temperatures. *Geochim. Cosmochim. Acta* 59, 1497–1532.
- Stumm, W., Morgan, J.J., 1996. *Aquatic Chemistry*. Wiley, New York.

- Suzuki, Y., Banfield, J.F., 1999. Geomicrobiology of uranium. Uranium, Mineralogy, Geochemistry and the Environment. Reviews in Mineralogy, vol. 38, Mineralogical Society of America, pp. 393–432.
- Taratus, E., Eubanks, S., DiChristina, T., 2000. Design and application of a rapid screening technique for isolation of selenite reduction-deficient mutants of *Shewanella putrefaciens*. Microbiol. Res. 155 (2), 79–85.
- Ticknor, K.V., Vilks, P., Vandergraaf, T.T., 1996. The effect of fulvic acid on the sorption of actinides and fission products on granite and selected minerals. Appl. Geochem. 11, 555–565.
- Tipping, E., Hurley, M.A., 1992. A unifying model of cation binding by humic substances. Geochimica et Cosmochimica Acta 56, 3627–3641.
- Tripathi, V.S., 1994. Uranium (VI) transport modeling: Geochemical data and submodels: Unpublished PhD Dissertation, Stanford Univ., Stanford, CA, 297 pp.
- Voet, D., Voet, J.G., 1995. Biochemistry. Wiley, New York.
- Wade Jr., R., DiChristina, T.J., 2000. Isolation of U(VI) reduction-deficient mutants of *Shewanella putrefaciens*. FEMS Microbiol. Lett. 184, 143–148.
- Wagman, D.D., Evans, W.H., Parker, V.B., Schumm, R.H., Halow, I., Bailey, S.M., Churney, K.L., Nuttall, R.L., 1982. The NBS tables of chemical thermodynamic properties. J. Phys. Chem. Ref. Data 11 (Supplement no. 2), 392 pp.
- Waite, T.D., Davis, J.A., Payne, T.E., Waychunas, G.A., Xu, N., 1994. Uranium(VI) adsorption to ferrihydrite: application of a surface complexation model. Geochim. Cosmochim. Acta 58, 5465–5478.
- Westall, J.C., 1982. FITEQL. A computer program for determination of chemical equilibrium constants from experimental data. Version 2.0. Report 82-02, Dept. of Chemistry, Oregon State University, Corvallis, OR.
- Winkler, A., Maue, G., Dott, W., Taute, T., Pekdeger, A., Stroetmann, I., 1995. Microbiological alteration of the transport behaviour of redoxsensitive radionuclides in sediments. Water–rock interaction. Proc. Symposium. Balkema, Vladivostok, pp. 277–280.
- Wolery, T.J., 1992. EQ3NR, a computer program for geochemical aqueous speciation–solubility calculations: theoretical manual, user's guide, and related documentation (version 7.0), Lawrence Livermore National Laboratory.